Optica Applicata, Vol. XLIX, No. 2, 2019
DOI: 10.5277/oa190206

Numerical analysis of dual-core photonic crystal fiber based temperature and pressure sensor for oceanic applications

SUBRAMANI JEGADEESAN[1*], MUNEESWARAN DHAMODARAN[1], SWAMINATHAN SRI SHANMUGAPRIYA[2]

[1]Department of Electronics and Communication Engineering, M. Kumarasamy College of Engineering, Karur 639113, Tamilnadu, India

[2]Department of Electronics and Communication Engineering, V.S.B. Engineering College, Karur 639111, Tamilnadu, India

[*]Corresponding author: jegadeesans@rediffmail.com

In this paper, a microstructured optical fiber with dual core was proposed which is known as photonic crystal fiber. Specific optical properties of a dual-core photonic crystal fiber were used to obtain high birefringence, small beat length, flattened dispersion, for different values of structural parameters varied over a wide range of wavelength and analyzed for application such as temperature and pressure sensors. The sensitivity of the temperature sensor is calculated as 20 pm/°C for 6 cm fiber, the sensitivity of the pressure sensor for a range from 0 to 1000 kPa is calculated as –10.5 nm/MPa.

Keywords: dual core, photonic crystal fiber, birefringence, temperature sensor, pressure sensor, finite element method.

1. Introduction

A new type of microstructured optical fiber is known as a photonic crystal fiber (PCF). It consists of very small and closely spread out air holes. In the PCF the lights are confined inside the silica tubes. Due to special properties of the PCF, they have attracted an attention which resulted in a number of researchers in the recent years. In [1] a new type of fiber to carry the light signal in a hollow core by photonic band gap cladding has been introduced. In [2] another type of PCF with a cladding structure of periodic air holes in silica has been proposed. The main parameters considered in designing a PCF are the diameter d of air holes and the distance between the centers of the two adjacent air holes D, and are shown in Fig. 1. Photonic crystal fibers are produced by a stack and draw method.

The PCF coupler is one of the important elements in the future optical networks [3–6]. Realization of a dual-core PCF allows us to design efficient PCF couplers, wave-

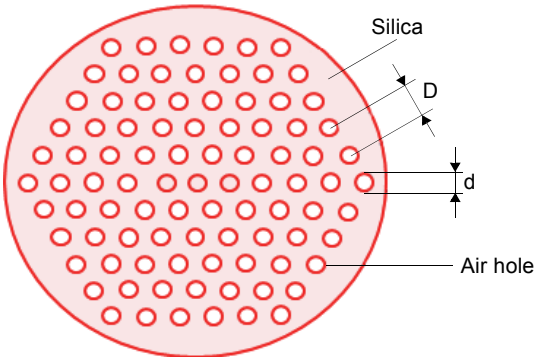

Fig. 1. Photonic crystal fiber structure.

length multiplexers and demultiplexers, splitters, filters and sensors [7–11]. When compared to conventional optical couplers, a dual-core PCF coupler has more advantages. That is, it is easy to design, is flexible and has small coupling wavelength. The important physical properties of a dual-core PCF are coupling length and birefringence. The main feature of this dual-core PCF is that it can be used as a temperature and pressure sensor in some applications.

For temperature measurements in basic metals and glass productions, in critical turbine areas, power generation operations, ovens, sintering operations rolling lines in steel furnaces, and in automated welding equipment (having large electrical fields), fiber optic sensors can be used. In applications as high temperature processing operations in cement and chemical industries, optical fibers based temperature measurement has proved to be quite efficient. Accordingly, temperature-based PCF sensors were developed to produce new sensors with improved characteristics, sensibility and stability. Studies influencing the geometry and the material quality in the high birefringent PCF sensitive to temperature were developed [12]. A polarimetric examination of this kind of high birefringent PCF confirmed a sensitivity of 0.136 rad/°C at 1310 nm [13].

The most recent approach to temperature measurements using PCFs is by inserting them in a hollow core of a PCF and filling them with liquid to attain a sensitivity of 70 pm/°C [14]. Solid core PCFs, air holes of the cladding are filled with nanoparticle fluid, and depending on the length of the fiber (from 5 to 10 cm), a temperature sensitivity of 0.045–0.06 dB/°C was achieved [15]. By filling 10 cm of solid-core PCFs with a less expensive liquid, like ethanol, a sensitivity of 0.315 dB/°C was reported [16]. On infiltrating one of the air holes of a solid-core PCF having a refractive index of 1.46, the sensitivity to temperature has been proved to be ~54.3 nm/°C [17].

In many industries with oil and gas exploitations, turbine engines, compressors, power plants and material processing systems, pressure measurements are required. Due to the high temperatures, corrosive agents or electromagnetic interference present in harsh environments conventional sensors are difficult to apply. Fiber optic pressure sensors have been proved to be effective in such environments as they possess high operation temperature, wide bandwidth, lightweight, high sensitivity, long life and are

immune to electromagnetic interference. Hydrostatic pressure up to 180 bar with a pressure sensitivity of 11.2 pm/bar can be measured using periodically tapered LPGs written in an endlessly single-mode PCF [18].

Polarimetric measurement is a popular technique for pressure sensing. Several authors reported the polarimetric studies and measurements leading to the development and application of pressure sensors based on the commercial Hi-Bi PCF, at three different temperatures. The study of pressure sensing with this PCF portrayed its temperature insensitivity, at the same time measuring pressure variations [19]. Intensity measurement of pressure with a sensitivity of 2.34×10^{-6} MPa^{-1} was later illustrated [20] and wavelength measurements of pressure variation showed a sensitivity of 3.38 nm/MPa at an operating limit of 92 MPa [21] which led to practical applications. Tsunami sensing, as the high pressure sensitivity along with temperature insensitivity, makes the sensor apt to work in a harsh environment such as the ocean bottom [22].

The main objective of this paper is to analyze physical properties of the dual-core PCF to obtain high birefringence, small beat length, and flattened dispersion for different values of structural parameters varied over a wide range of wavelength and analyzed from the point of view of potential applications like temperature and pressure sensors.

2. Proposed dual-core PCF design

The proposed dual-core PCF structure is shown in Fig. 2. Here, D represents the distance between the centers of two adjacent air holes and d represents the diameter of an air hole. The proposed structure consists of 1.40 μm diameter of air holes and 2.2 μm distance between the centers of the air holes.

In a dual-core PCF, the two cores are surrounded by 10 air holes. The proposed structure is analyzed for two different situations. First, the proposed PCF is analyzed by keeping an air hole diameter of 1.40 μm as constant and changing the D value. In the second case, the distance between the center of air holes D is constant and changing

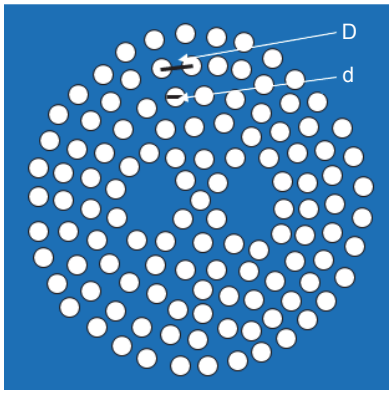

Fig. 2. Dual-core photonic crystal fiber.

the diameter d value. Different d/D values are considered for analyzing the proposed dual-core PCF structure in the two cases. Figure 2 shows the light captivity electric field x-polarized even mode. The proposed dual-core PCF is made up of silica material with a refractive index value of 1.45. Figure 3 shows the light captivity electric field x-polarized even mode. Also Fig. 3 shows the two- and three-dimensional light captivity diagrams.

The light gets confined into two cores for each wavelength. The effective indices for wavelength in the range from 0.85 to 1.65 μm are noted for x-polarized light even and odd modes and y-polarized light even and odd modes from the simulated structure. The polarized lights are differentiated based on the direction of the electric field.

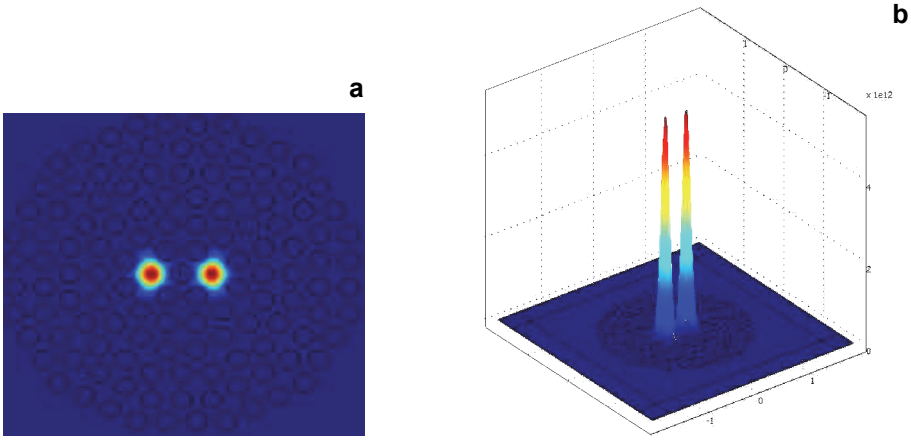

Fig. 3. Simulated structure of PCF. Two-dimensional (**a**) and three-dimensional (**b**) representation of simulated PCF.

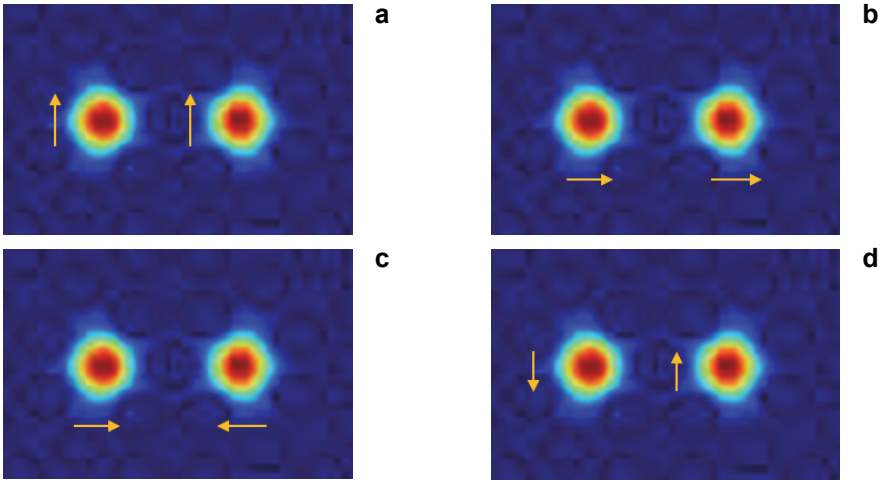

Fig. 4. Field distribution: y-polarized (even mode) (**a**), x-polarized (even mode) (**b**), x-polarized (odd mode) (**c**), and y-polarized (odd mode) (**d**).

T a b l e 1. Parameter values for different structures in two cases.

	Case 1: constant d, different D		Case 2: constant D, different d	
d/D	d [μm]	D [μm]	d [μm]	D [μm]
0.5	1.40	2.71	1.0	2.0
0.6	1.40	2.55	1.2	2.0
0.7	1.40	2.13	1.4	2.0
0.8	1.40	1.82	1.6	2.0
0.9	1.40	1.54	1.8	2.0

Figure 4 shows four different modes for the electric field profile of x- and y-polarized mode. Two arrows pointing in opposite directions denote the odd mode and in the same direction even mode. The structure is simulated for different structural parameters. The structure is simulated using a finite element method for different d/D values of 0.5, 0.6, 0.7, 0.8 and 0.9 and the properties are analyzed.

Effective index, birefringence, beat length and chromatic dispersion are discussed for a broad wavelength range from 0.85 to 1.65 μm. The structure with d/D of 0.7 is considered as common in both scenarios and discussed. Table 1 shows the structural parameters for two different cases to be discussed. Case 1 with constant d and varied D and case 2 with constant D and varied d.

3. Analysis of optical properties of dual-core PCF

3.1. Effective index

The proposed PCF structure produces a strong wavelength and it is different from silica material. It permits to design a new PCF with new features differing from the existing methods. Figures 5 and 6, explain the first and second case, respectively, which indi-

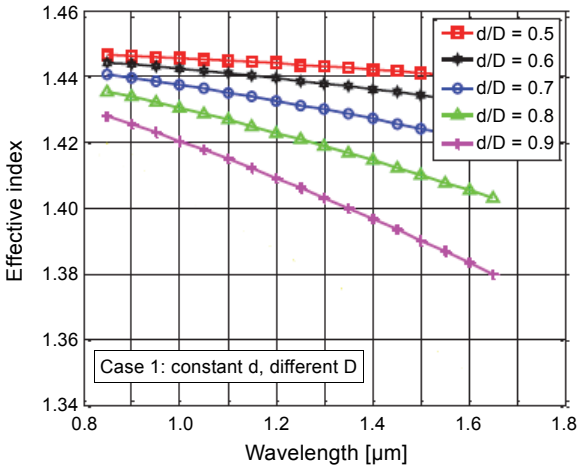

Fig. 5. Variation of effective index with wavelength for case 1.

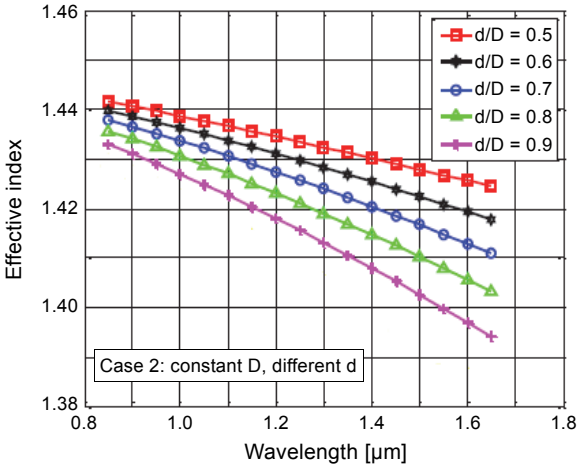

Fig. 6. Variation of effective index with wavelength for case 2.

T a b l e 2. Effective index for case 1 and case 2 at 1.55 μm.

	Effective index (n_x even)				
	$d/D = 0.5$	$d/D = 0.6$	$d/D = 0.7$	$d/D = 0.8$	$d/D = 0.9$
Case 1 (d = 1.40 μm)	1.429356	1.425397	1.408345	1.391286	1.349371
Case 2 (D = 2.0 μm)	1.421751	1.417419	1.409392	1.388571	1.352859

cates the changes in the effective mode index with wavelength. It is observed that, when the wavelength is increased, the value of the effective index decreases because at higher wavelength light confinement is weak. In Fig. 5, D is varied and diameter d is kept constant for different values of d/D, and Fig. 6 shows the variation of the effective index with wavelength for different d/D ratios when the diameter d is varied and D is kept constant.

At a wavelength of 1.55 μm, when d/D value is increased, the effective index is decreased. At 1.55 μm, the effective index for x-polarized light is 1.408345 and for y-polarized light is 1.409392 for d/D of 0.7. Table 2 shows the effective index for case 1 and case 2 at 1.55 μm for different d/D values.

3.2. Birefringence

Birefringence is defined as the difference between the propagation constants or mode indices of the slow and the fast polarization modes. Birefringence is the difference between the mode indices of the orthogonally polarized modes

$$B = \left|\mathrm{Re}(n_{\mathrm{ei}}^{x}) - \mathrm{Re}(n_{\mathrm{ei}}^{y})\right| \tag{1}$$

where n_{ei}^{x} and n_{ei}^{y} are effective indices in the x- and y-polarized directions, respectively. Figures 7 and 8 explain the proposed dual-core PCF birefringence for the two

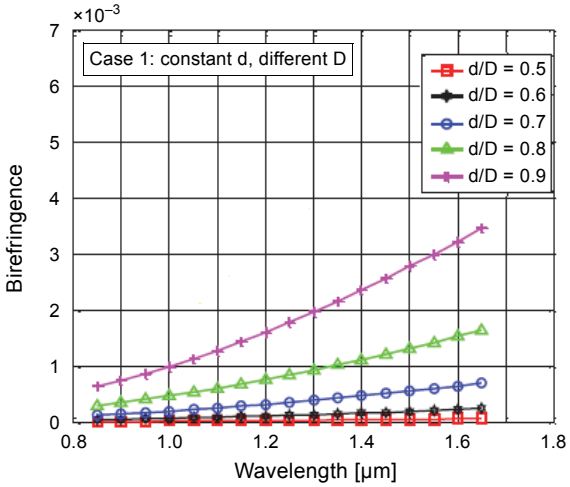

Fig. 7. Birefringence varying with wavelength for case 1.

different cases with different wavelength. In Fig. 7, the birefringence decreases with an increase in the D.

When D increases, the core area of fiber gets increased and the contact between inner holes and mode fields gets reduced. As D increases with a fixed air holes diameter, birefringence decreases with corresponding d/D ratio. For any specific d/D ratio, birefringence increases with wavelength.

Figure 7 shows that, by increasing the diameter of the air holes, the leaping capability of cladding becomes strong and the control of inner holes irregularity on light field rises, therefore the birefringence also increases. When d of air holes increases with constant D, d/D ratio increases and also increases the birefringence. At 1.55 μm,

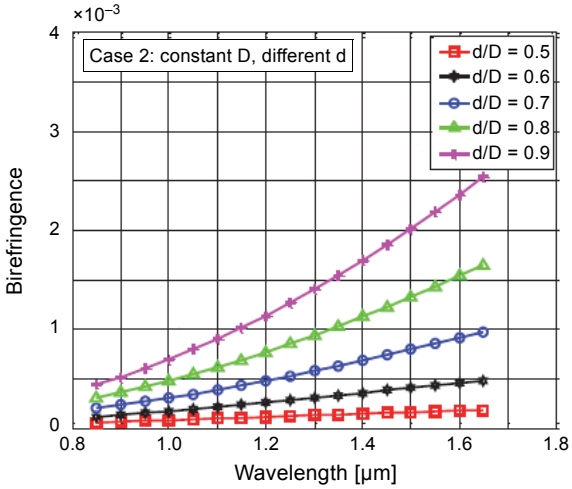

Fig. 8. Birefringence varying with wavelength for case 2.

T a b l e 3. Birefringence for case 1 and case 2 at 1.55 μm.

	Birefringence				
	$d/D = 0.5$	$d/D = 0.6$	$d/D = 0.7$	$d/D = 0.8$	$d/D = 0.9$
Case 1 (d = 1.40 μm)	2.19×10^{-4}	6.15×10^{-4}	1.59×10^{-3}	2.99×10^{-3}	6.01×10^{-3}
Case 2 (D = 2.0 μm)	4.58×10^{-4}	7.98×10^{-4}	1.73×10^{-3}	2.21×10^{-3}	3.17×10^{-3}

the birefringence is in the order of 10^{-3} for d/D of 0.7 which is good as compared to birefringence [23]. From Figs. 7 and 8, it is very clear that when d/D ratio is increased, birefringence also gets increased. For higher d/D ratio, high birefringence is obtained. If birefringence is higher, then the x- and y-polarized light splits from each other at a certain length of fiber and it can be realized as a splitter. Table 3 shows the birefringence for case 1 and case 2 at 1.55 μm.

3.3. Beat length

The beat length of the fiber is calculated by using the following equation:

$$L_{\mathrm{bl}} = \lambda / B \ [\mu\mathrm{m}] \tag{2}$$

where λ and B represent the wavelength and birefringence of the fiber [24]. Beat length variations with wavelength for two different cases are shown in Figs. 9 and 10.

High birefringence can eliminate the fluctuation in polarization state and hence the coupling from one polarization to other is difficult. Lesser value of beat length indicates the larger value of birefringence and therefore, the fiber having high polarization holding ability. As polarization holding ability is measured in terms of beat length, at higher birefringence, smaller beat length is obtained which results in no significant effect on

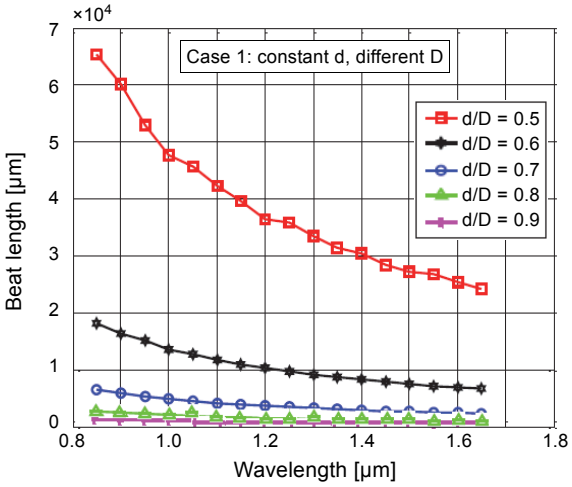

Fig. 9. Beat length varying with wavelength for case 1.

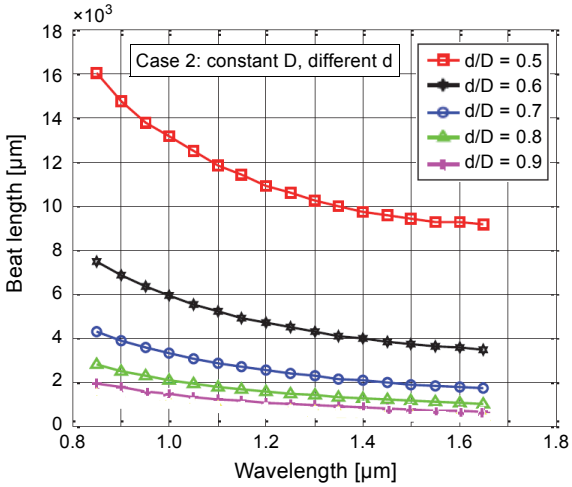

Fig. 10. Beat length varying with wavelength for case 2.

T a b l e 4. Beat length for case 1 and case 2 at 1.55 μm.

	Beat length [mm]				
	$d/D = 0.5$	$d/D = 0.6$	$d/D = 0.7$	$d/D = 0.8$	$d/D = 0.9$
Case 1 (d = 1.40 μm)	7.5801	2.7529	1.1052	0.6001	0.3173
Case 2 (D = 2.0 μm)	3.0586	1.9052	1.1052	0.8085	0.5194

polarization state. The fiber with high birefringence has a typical value of beat length in the range from 1 to 2 mm. As birefringence is high and of the order of 10^{-3}, smaller beat length at 1.55 μm is observed.

For d/D = 0.5, the beat length is 7.508 mm for the first case and 3.0586 mm for the second case at 1.55 μm. But when we increase the d/D ratio to 0.7, we get a very small beat length of 1.1052 mm at 1.55 μm wavelength as birefringence is high, *i.e.* 1.43×10^{-3}. Table 4 shows the beat length for the case 1 and case 2 at 1.55 μm.

3.4. Chromatic dispersion

Chromatic dispersion plays an important role in governing the pulse width and peak intensity evolving along the fiber length. Chromatic dispersion includes material dispersion and waveguide dispersion [25]. Material dispersion refers to the wavelength dependence of the refractive index of a material caused by the interaction between the light and ions, molecules or electrons in the material. Chromatic dispersion curves for different d/D values are plotted and shown in Figs. 11 and 12. This includes material dispersion. The dispersion centered near 1.55 μm has positive dispersion of +54.15 ps/nm · km for case 1 and flattened dispersion of –0.887 to +31.05 s/nm · km for case 2 within the wavelength range of 1.20–1.70 μm for d/D = 0.5 at 1.55 μm. It increases as d/D value

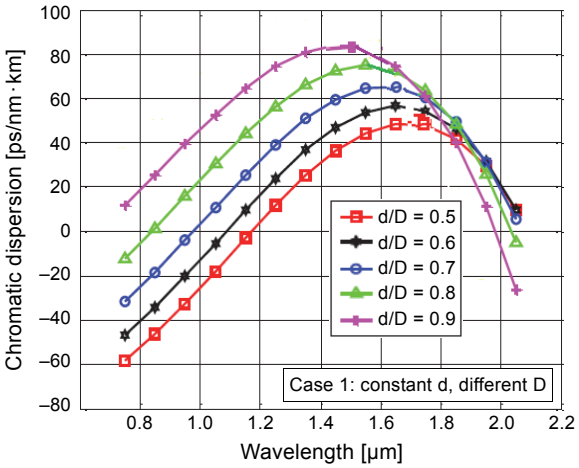

Fig. 11. Chromatic dispersion for D (different) and d (constant).

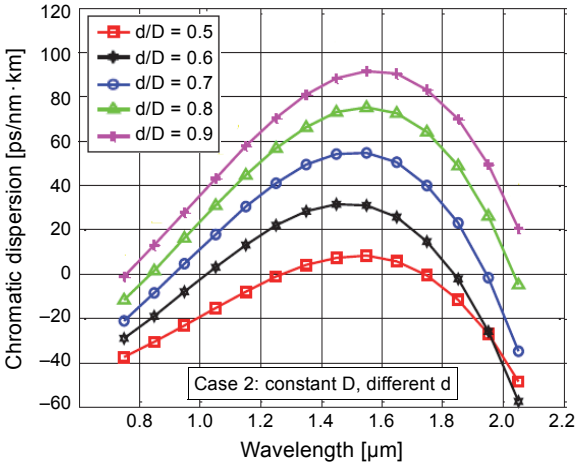

Fig. 12. Chromatic dispersion for d (different) and D (constant).

increases and reaches to a flattened dispersion of –4.8780 to +76.0165 ps/nm · km over a wide wavelength range of 0.80 to 2.1 μm when d/D is 0.7. It can be seen from Figs. 11 and 12 that two zero dispersion is obtained for most of the cases.

T a b l e 5. Dispersion value for case 1 and case 2 at 1.55 μm.

	Dispersion [ps/nm · km]				
	$d/D = 0.5$	$d/D = 0.6$	$d/D = 0.7$	$d/D = 0.8$	$d/D = 0.9$
Case 1 (d = 1.40 μm)	54.15	65.31	76.0165	81.98	80.94
Case 2 (D = 2.0 μm)	31.05	55.06	76.0165	92.29	105.01

When the size of the air holes increases, two zero dispersion is observed for all d/D ratios. The non-zero flattened dispersion is obtained at a lower value of $d = 0.8$ μm over a wavelength range from 1.20 to 1.70 μm but as the diameter of air holes increases, flattened dispersion is obtained with a higher value, as shown in Fig. 12. While D increases in the first case, two zero dispersion occurs at d/D ratio of 0.7 as shown in Fig. 11. When D is varied with constant diameter of air holes, flattened dispersion is noticed but with a higher value. Table 5 illustrates the dispersion value for case 1 and case 2 at 1.55 μm.

4. Dual core PCF based temperature and pressure sensor

When pressure or air is applied on the silica fiber, it changes the refractive index of the fiber. Variations in the refractive index is given by

$$n_a = n_0 - c_1 v_x - c_2(v_y - v_z) \tag{3}$$

$$n_b = n_0 - c_1 v_y - c_2(v_x - v_z) \tag{4}$$

Here v_x, v_y and v_z are the variables used to define the pressure; $c_1 = 6.5 \times 10^{-13}$ m^2/N and $c_2 = 4.2 \times 10^{-12}$ m^2/N are pressure coefficients of the silica material. FEM analysis is used to find the pressure in the silica material. When pressure is applied on the dual core PCF, it leads to changes in the refractive index difference Δn_{21}. When pressure is applied on the dual core PCF, due to the strain optic effect, it will change the refractive index of the fiber and it will lead to variations in the spectrum transmission [26].

When fiber is subjected to temperature, it changes the refractive index of the fiber because of the thermo-optic effect [27, 28]. The silica material thermo-optic coefficient is 10^{-5}/°C. When temperature t is applied, the refractive index of the fiber is given by $n_t = 1.5 + 10^{-5} t$. That is, based on the temperature, the refractive index of the dual core PCF will get varied. When temperature is applied on the fiber, it leads to variation in the refractive index difference Δn_{21}. Hence, there is a change in the dual core PCF and transmission spectrum depends on the applied temperature.

The dual core PCF spectral variation depends on the applied temperature which is shown in Fig. 13. The spectral variation is observed when the dual core PCF is subjected to different temperature values. At very high temperature, there is a spectral variation in the longer wavelength due to the small refractive index difference. When the fiber surrounding temperature increases, the fiber transmission curve moves to the right side. It gives the full spectra for general operation.

There is a change in the peak wavelength under different temperature values from 0 to 1000°C. When temperature increases, there is a large variation in the peak wavelength and it is shown in Fig. 14. From Fig. 14, it is observed that the transmission curve of the fiber gets varied by 5 nm for every 200°C. Therefore, the sensitivity of the fiber sensor is calculated as 20 pm/°C for 6 cm fiber.

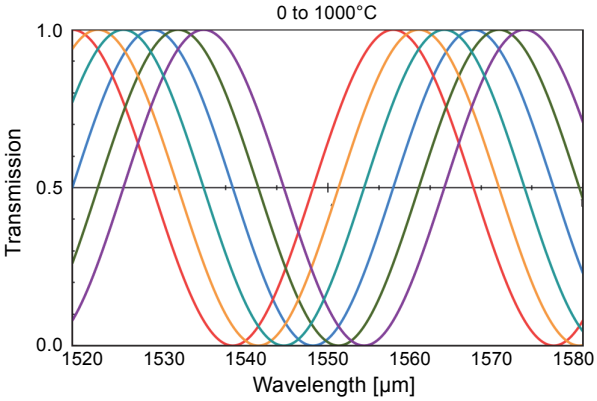

Fig. 13. Dual core PCF transmission spectra for different temperatures.

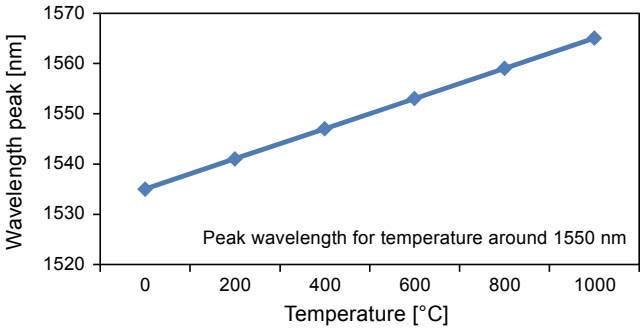

Fig. 14. Peak wavelength changes for different temperatures.

When fiber is subjected to different temperature values, the size and properties of the fiber are changed. These changes are observed in birefringence. Variations in birefringence for different temperature values at 1550 nm are shown in Fig. 15. It is observed that there is a linear variation in birefringence with respect to the increase in temperature. The transmission spectra of the dual core PCF for different pressure levels

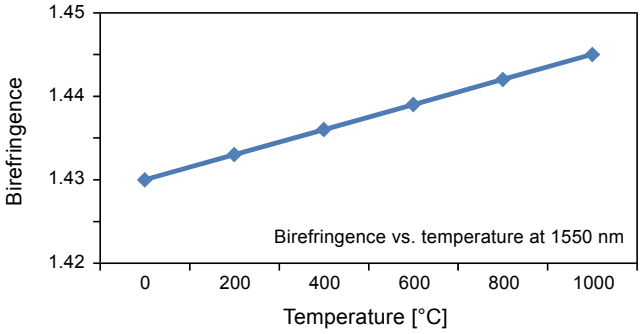

Fig. 15. Birefringence changes for different temperatures at 1550 nm.

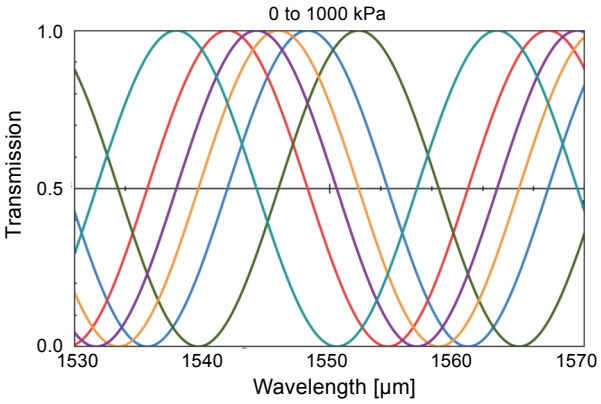

Fig. 16. Dual core PCF transmission spectra for different pressure values.

are shown in Fig. 16. The transmission curve moves to the left when applied pressure increases.

When fiber is subjected to different pressure levels, there is a change in the peak of transmission curve. When pressure is applied to both sides of the fiber, the transmission curve of the fiber moves to a lower wavelength. From Fig. 17, it is observed that the

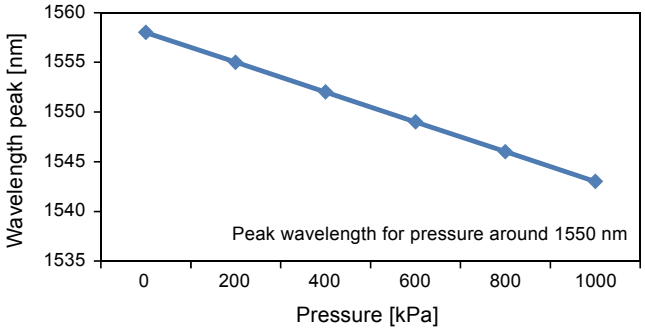

Fig. 17. Peak wavelength changes for different pressure values.

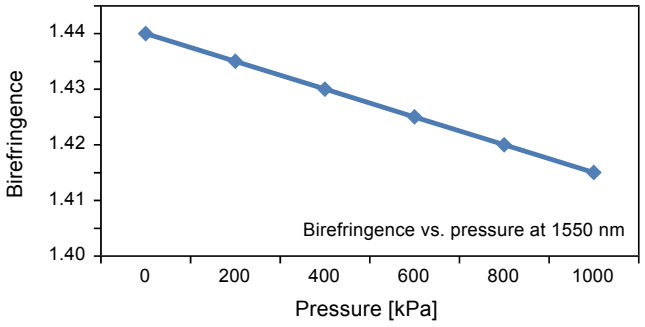

Fig. 18. Birefringence changes for different pressure values at 1550 nm.

Table 6. Comparison of the proposed dual-core PCF based temperature and pressure sensor with existing works.

Method	Sensitivity of pressure sensor	Method	Sensitivity of temperature sensor
Pandey's scheme [29]	5.3/MPa	Yu Yongoin's scheme [16]	8.17 pm/°C
Pandey's scheme [30]	3.0×10^6 Pa	Ju's scheme [13]	42.4 pm/°C
Shinde's scheme [22]	3.24 nm/MPa	Geng's scheme [27]	71.5 pm/°C
Proposed scheme	–10.5 nm/MPa	Proposed scheme	20 pm/°C

peak transmission curve moves to a lower wavelength of 2.0 nm for every 200 kPa pressure value. Hence, the sensitivity of the fiber sensor is calculated as –10.5 nm/MPa. Figure 18 explains the variations in the birefringence for different pressure values. It is observed that there is a linear decrease in birefringence values with respect to different pressure values from 0 to 1000 kPa at 1550 nm. From these results it is clear that the proposed dual-core PCF based temperature and pressure sensor perform well as compared with existing works [27–30]. The comparison of the proposed dual-core PCF based temperature and pressure sensor with the existing works is shown in Table 6.

5. Conclusion

A dual-core PCF was designed in this study. In addition, its physical properties were analyzed to obtain high birefringence, small beat length, and flattened dispersion for different values of structural parameters varied over a wide range of wavelength and analyzed for applications such as temperature and pressure sensors. The sensitivity of the temperature sensor was calculated as 20 pm/°C for 6 cm fiber, and the sensitivity of the pressure sensor was calculated as –10.5 nm/MPa. The proposed dual-core PCF structure was found to have more pressure sensitivity and less temperature sensitivity. Hence, the proposed fiber structure can be used in oceanic applications.

References

[1] ASADUZZAMAN S., AHMED K., *Proposal of a gas sensor with high sensitivity, birefringence and non-linearity for air pollution monitoring*, Sensing and Bio-Sensing Research **10**, 2016, pp. 20–26, DOI: 10.1016/j.sbsr.2016.06.001.

[2] WEI SU, SHUQIN LOU, HUI ZOU, BOLIN HAN, *A highly nonlinear photonic quasi-crystal fiber with low confinement loss and flattened dispersion*, Optical Fiber Technology **20**(5), 2014, pp. 473–477, DOI: 10.1016/j.yofte.2014.05.016.

[3] YASLI A., ADEMGIL H., *Geometrical comparison of photonic crystal fiber-based surface plasmon resonance sensors*, Optical Engineering **57**(3), 2018, article ID 030801, DOI: 10.1117/1.OE.57.3.030801.

[4] HAIWEI ZHANG, LIANGCHENG DUAN, WEI SHI, QUAN SHENG, YING LU, JIANQUAN YAO, *Dual-point automatic switching intracavity-absorption photonic crystal fiber gas sensor based on mode competition*, Sensors and Actuators B: Chemical **247**, 2017, pp. 124–128, DOI: 10.1016/j.snb.2017.03.007.

[5] PINTO A.M.R., LOPEZ-AMO M., *Photonic crystal fibers for sensing applications*, Journal of Sensors, Vol. 2012, 2012, article ID 598178, DOI: 10.1155/2012/598178.

[6] ISLAM F., HAQUE A., *Analysis of Hexagonal & Spiral Photonic Crystal Fiber (PCF) using Finite Element Method*, A thesis submitted in partial fulfillment of the requirements for the degree *Bachelor of Science in Electrical and Electronic Engineering*, Department of Electrical and Electronic Engineering, Bangladesh University of Engineering and Technology (BUET), 2013, DOI: 10.13140/RG.2.1.1145.8323.

[7] ISLAM I., PAUL B.K., AHMED K., HASAN R., CHOWDHURY S., ISLAM S., SEN S., BAHAR A.N., ASADUZZAMAN S., *Highly birefringent single mode spiral shape photonic crystal fiber based sensor for gas sensing applications*, Sensing and Bio-Sensing Research **14**, 2017, pp. 30–38, DOI: 10.1016/j.sbsr.2017.04.001.

[8] STASIEWICZ K.A., MUSIAL J.E., *Threshold temperature optical fibre sensors*, Optical Fiber Technology **32**, 2016, pp. 111–118, DOI: 10.1016/j.yofte.2016.10.009.

[9] GUOCHEN WANG, ZHENPENG WANG, FEI YU, *Design of single-polarization single-mode coupler based on dual-core photonic crystal fiber*, Optical Engineering **55**(2), 2016, article ID 027101, DOI: 10.1117/1.OE.55.2.027101.

[10] IBRAHIM A., POULON F., MELOUKI F., ZANELLO M., VARLET P., HABERT R., DEVAUX B., KUDLINSKI A., ABI HAIDAR D., *Spectral and fluorescence lifetime endoscopic system using a double-clad photonic crystal fiber*, Optics Letters **41**(22), 2016, pp. 5214–5217, DOI: 10.1364/OL.41.005214.

[11] MAO LIU, JIAWEI XIANG, YONGTENG ZHONG, *Band structures analysis method of two-dimensional phononic crystals using wavelet-based elements*, Crystals **7**(11), 2017, pp. 328–336, DOI: 10.3390/cryst7110328.

[12] MARTYNKIEN T., SZPULAK M., URBANCZYK W., *Modeling and measurement of temperature sensitivity in birefringent photonic crystal holey fibers*, Applied Optics **44**(36), 2005, pp. 7780–7788, DOI: 10.1364/AO.44.007780.

[13] JIAN JU, ZHI WANG, WEI JIN, DEMOKAN M.S., *Temperature sensitivity of a two-mode photonic crystal fiber interferometric sensor*, IEEE Photonics Technology Letters **18**(20), 2006, pp. 2168–2170, DOI: 10.1109/LPT.2006.883889.

[14] BOZOLAN A., GEROSA R.M., DE MATOS C.J.S., ROMERO M.A., *Temperature sensing using colloidal-core photonic crystal fiber*, IEEE Sensors Journal **12**(1), 2012, pp. 195–200, DOI: 10.1109/JSEN.2011.2146771.

[15] YINPING MIAO, BO LIU, KAILIANG ZHANG, YAN LIU, HAO ZHANG, *Temperature tunability of photonic crystal fiber filled with Fe_3O_4 nanoparticle fluid*, Applied Physics Letters **98**(2), 2011, article ID 021103, DOI: 10.1063/1.3540647.

[16] YONGQIN YU, XUEJIN LI, XUEMING HONG, YUANLONG DENG, KUIYAN SONG, YOUFU GENG, HUIFENG WEI, WEIJUN TONG, *Some features of the photonic crystal fiber temperature sensor with liquid ethanol filling*, Optics Express **18**(15), 2010, pp. 15383–15388, DOI: 10.1364/OE.18.015383.

[17] YING WANG, MINWEI YANG, WANG D.N., LIAO C.R., *Selectively infiltrated photonic crystal fiber with ultrahigh temperature sensitivity*, IEEE Photonics Technology Letters **23**(20), 2011, pp. 1520–1522, DOI: 10.1109/LPT.2011.2163705.

[18] BOCK W.J., CHEN J., MIKULIC P., EFTIMOV T., KORWIN-PAWLOWSKI M., *Pressure sensing using periodically tapered long-period gratings written in photonic crystal fibres*, Measurement Science and Technology **18**(10), 2007, pp. 3098–3102, DOI: 10.1088/0957-0233/18/10/S08.

[19] BOCK W.J., CHEN J., EFTIMOV T., URBANCZYK W., *A photonic crystal fiber sensor for pressure measurements*, IEEE Transactions on Instrumentation and Measurement **55**(4), 2006, pp. 1119–1123, DOI: 10.1109/TIM.2006.876591.

[20] GAHIR H.K., KHANNA D., *Design and development of a temperature-compensated fiber optic polarimetric pressure sensor based on photonic crystal fiber at 1550 nm*, Applied Optics **46**(8), 2007, pp. 1184–1189, DOI: 10.1364/AO.46.001184.

[21] FÁVERO F.C., QUINTERO S.M.M., MARTELLI C., BRAGA A.M.B., SILVA V.V., CARVALHO I.C.S., LLERENA R.W.A., VALENTE L.C.G., *Hydrostatic pressure sensing with high birefringence photonic crystal fibers*, Sensors, **10**(11), 2010, pp. 9698–9711, DOI: 10.3390/s101109698.

[22] SHINDE Y.S., GAHIR H.K., *Dynamic pressure sensing study using photonic crystal fiber: application to tsunami sensing*, IEEE Photonics Technology Letters **20**(4), 2008, pp. 279–281, DOI: 10.1109/LPT.2007.913741.

[23] FEIFEI SHI, YUN WU, MEICHENG LI, YU ZHAO, LIANCHENG ZHAO, *Highly birefringent two-mode photonic crystal fibers with near-zero flattened dispersion*, IEEE Photonics Journal **3**(6), 2011, pp. 1181–1188, DOI: 10.1109/JPHOT.2011.2176480.

[24] SARMA V., SHARMA R., *Design of hybrid photonic crystal fiber with elliptical and circular air holes analyzed for large flattened dispersion and high birefringence*, Journal of Nanophotonics **10**(2), 2016, article ID 026016, DOI: 10.1117/1.JNP.10.026016.

[25] KOOHI-KAMALI F., EBNALI-HEIDARI M., MORAVVEJ-FARSHI M.K., *Designing a dual-core photonic crystal fiber coupler by means of microfluidic infiltration*, International Journal of Optics and Photonics **6**(2), 2012, pp. 83–96.

[26] DARU CHEN, GUFENG HU, LINGXIA CHEN, *Dual-core photonic crystal fiber for hydrostatic pressure sensing*, IEEE Photonics Technology Letters **23**(24), 2011, pp. 1851–1853, DOI: 10.1109/LPT.2011.2170194.

[27] YOUFU GENG, XUEJIN LI, XIAOLING TAN, YUANLONG DENG, YONGQIN YU, *Sensitivity-enhanced high -temperature sensing using all-solid photonic bandgap fiber modal interference*, Applied Optics **50**(4), 2011, pp. 468–472, DOI: 10.1364/AO.50.000468.

[28] WENWEN QIAN, CHUN-LIU ZHAO, SHAOLING HE, XINYONG DONG, SHUQIN ZHANG, ZAIXUAN ZHANG, SHANGZHONG JIN, JIANGTAO GUO, HUIFENG WEI, *High-sensitivity temperature sensor based on an alcohol-filled photonic crystal fiberloop mirror*, Optics Letters **36**(9), 2011, pp. 1548–1550, DOI: 10.1364/OL.36.001548.

[29] PANDEY N.K., YADAV B.C., *Fibre optic pressure sensor and monitoring of structural defects*, Optica Applicata **37**(1–2), 2007, pp. 57–63.

[30] PANDEY N.K., YADAV B.C., *Embedded fibre optic microbend sensor for measurement of high pressure and crack detection*, Sensors and Actuators A: Physical **128**(1), 2006, pp. 33–36, DOI: 10.1016/j.sna.2006.01.010.

Received April 25, 2018
in revised form June 18, 2018